Two-dimensional excitons from twisted light and the fate of the photon's orbital angular momentum

Tobias Graß,[1] Utso Bhattacharya,[1] Julia Sell,[2] and Mohammad Hafezi[2,3]
[1]*ICFO-Institut de Ciencies Fotoniques, The Barcelona Institute of Science and Technology, 08860 Castelldefels (Barcelona), Spain*
[2]*Joint Quantum Institute, NIST and University of Maryland, College Park, Maryland 20742, USA*
[3]*Department of Electrical Engineering and Institute for Research in Electronics and Applied Physics, University of Maryland, College Park, Maryland 20742, USA*

(Received 1 February 2022; revised 29 April 2022; accepted 3 May 2022; published 12 May 2022)

As the bound state of two oppositely charged particles, excitons emerge from optically excited semiconductors as the electronic analog of a hydrogen atom. In the two-dimensional (2D) case, realized in either quantum well systems or truly 2D materials such as transition metal dichalcogenides, the relative motion of an exciton is described by two quantum numbers: the principal quantum number n, and a quantum number j for the angular momentum along the perpendicular axis. Conservation of angular momentum demands that only the $j = 0$ states of the excitons are optically active in a system illuminated by plane waves. Here, we consider the case for spatially structured light sources, specifically for twisted light beams with nonzero orbital angular momentum per photon. Under the so-called dipole approximation where the spatial variations of the light source occur on length scales much larger than the size of the semiconductor's unit cell, we show that the photon (linear and/or angular) momentum is coupled to the center-of-mass (linear and/or angular) momentum of the exciton. Thus our study establishes that the exciton spectrum is independent from the spatial structure of the light source.

DOI: 10.1103/PhysRevB.105.205202

I. INTRODUCTION

Excitons are the bound states formed by an electron-hole pair in a semiconductor crystal [1,2], and as such, they are close analogs of the hydrogen atom. Excitons manifest themselves as optical absorption or emission lines within the band gap of the material. In the theoretical treatment of exciton formation, light-matter interaction is most often described within the dipole approximation. This approximation disregards the spatial structure of the light field, which is justified by the tiny length scale on which the de Broglie waves vary, as compared with the wavelength of the light [3].

The dipole approximation gives rise to certain optical selection rules related to the conservation of angular momentum during an optical transition. Within the dipole approximation, light may carry only one quantum of angular momentum per photon, realized through the circular polarization of the light; therefore optical transitions can change angular momentum quantum numbers of the matter only by one unit. In atoms, this rule selects the s-to-p or p-to-d transitions; in semiconductors, the selection rule affects the orbitals of the bands in an analogous way. As a consequence of the dipole approximation, excitons created from such a dipole transition do not carry angular momentum; that is, the respective quantum number j is zero. Moreover, as established by the Elliott formula [4], the transition amplitude quickly decays with the principal quantum n [as $(n + 1/2)^{-3}$ in two dimensions (2D)], such that the exciton spectrum is strongly dominated by transitions into the $1s$ state, i.e., the state corresponding to the hydrogenic ground state. A common technique to allow optical access to the p exciton series in semiconductors is nonlinear, two-photon spectroscopy [5,6].

It is clear that effects beyond the dipole approximation can modify the exciton spectrum. In particular, the dipole approximation disregards the possible spatial structure of the light beam, which in the case of twisted light results in a well-defined orbital angular moment (OAM) per photon [7–9]. The photon OAM essentially adds another tunable degree of freedom for tailoring light-matter interaction. It has been proposed to use this new degree of freedom for generating a topological band structure by breaking time-reversal symmetry [10], for pumping electrons in a magnetic field through the Landau level [11–13], or for producing topological defects such as vortices or skyrmions [14–17]. A striking demonstration of how the optical spectrum can be modified by photon OAM has been achieved in an experiment with trapped ions [18], showing a dipole-forbidden atomic s-to-d transition in the presence of a twisted light field. Given the analogy between an exciton and a hydrogen atom, it might be expected that twisted light can generate transitions into dark excitonic levels, where the photonic OAM is absorbed in the internal degree of freedom. This indeed has theoretically been suggested for the case of Rydberg excitons [19]. On the other hand, there have also been experiments with atomic and polaritonic condensates in which twisted light has led to the formation of vortices [20,21]. This indeed would suggest that the orbital angular momentum of the photon is absorbed by the center-of-mass (c.m.) degree of freedom of the exciton, rather than by the relative motion of electron and hole. Also, in the strong-drive limit and in the absence of Coulomb binding, OAM of light can lead to Floquet vortex creation, but it is an open question how strong drive and exciton formation compete with each other.

To better understand the fate of the photonic OAM in excitonic transitions, this paper studies the case of a single exciton in a two-band semiconductor model in 2D in the presence of a twisted light source. We extend theoretical studies of band-to-band transitions in semiconductors or graphene with twisted light, presented in Refs. [22–24], to the case where Coulomb interactions give rise to exciton formation. Our analysis demonstrates that, under the assumption that the spatial variation of the light occurs on a length scale much larger than the size of the unit cell of the semiconductor crystal, transitions into excitonic levels $j \neq 0$ remain completely forbidden even in the presence of twisted light. Instead, the structure of the light field selects the c.m. degree of freedom of the excitons. Since it is the relative motion that essentially determines the energy of an exciton, it follows that the twist of the light source does not modify the excitonic spectrum. In this context, we also note that small shifts of the spectrum are possible if the c.m. dispersion of the exciton is taken into account. This indeed has been observed in a recent experiment with excitons in a Dirac material, which found a blueshift of the exciton lines for sufficiently large values of photon OAM [25].

This paper is organized in the following way: In Sec. II, we develop the general analytical formalism to describe exciton transitions in structured light beam. In Sec. III, we specifically address the case of a Bessel beam. To evaluate this case, we make use of the rotational symmetry of the beam, which makes an explicit numerical treatment feasible. With this we are able to show, for a finite system size, that the s states are optically bright, in quantitative good agreement with the 2D Elliott formula, independent from the choice of the photon OAM. Our numerical calculation also confirms that the c.m. momentum of the exciton is peaked at the linear momentum of the photon.

II. GENERAL ANALYTICAL MODEL

A. Light-matter coupling

We consider a 2D semiconductor with Bloch bands λ and wave vector $\mathbf{k}$, described by Bloch functions $\varphi_{\lambda,\mathbf{k}}(\mathbf{r}) = \frac{1}{\sqrt{S}} e^{i\mathbf{k}\cdot\mathbf{r}} u_{\lambda,\mathbf{k}}(\mathbf{r})$, where $u_{\lambda,\mathbf{k}}(\mathbf{r}+\mathbf{R_i}) = u_{\lambda,\mathbf{k}}(\mathbf{r})$ with $\mathbf{R}_i$ being a lattice vector. In this basis, the crystal Hamiltonian reads $H_0 = \sum_{\lambda,\mathbf{k}} \epsilon_{\lambda,\mathbf{k}} c^\dagger_{\lambda,\mathbf{k}} c_{\lambda,\mathbf{k}}$, with $c_{\lambda,\mathbf{k}}$ ($c^\dagger_{\lambda,\mathbf{k}}$) being the annihilation (creation) operators and $\epsilon_{\lambda,\mathbf{k}}$ being the dispersion. We assume a light field given by a vector potential $\mathbf{A}(\mathbf{r}) = A(\mathbf{r})\cdot\mathbf{e}$ in the Coulomb gauge, such that the light-matter Hamiltonian is given by

$$H_{\mathrm{LM}} = \sum_{\lambda',\lambda}\sum_{\mathbf{k}',\mathbf{k}} \frac{ie\hbar}{M} \langle \lambda', \mathbf{k}'|\mathbf{A}(\mathbf{r})\cdot\nabla_{\mathbf{r}}|\lambda,\mathbf{k}\rangle c^\dagger_{\lambda',\mathbf{k}'} c_{\lambda,\mathbf{k}}. \quad (1)$$

We are only interested in the matrix element $h^{\lambda',\lambda}_{\mathbf{k}',\mathbf{k}} = (ie\hbar/M)\langle\lambda',\mathbf{k}'|\mathbf{A}(\mathbf{r})\cdot\nabla_{\mathbf{r}}|\lambda,\mathbf{k}\rangle = \int (ie\hbar/M) d^2r \varphi^*_{\lambda',\mathbf{k}'}(\mathbf{r})$ $A(\mathbf{r})\mathbf{e}\cdot\nabla_{\mathbf{r}}\varphi_{\lambda,\mathbf{k}}(\mathbf{r})$ with $\lambda = \mathrm{c}$ and $\lambda' = \mathrm{v}$, i.e., amplitudes of transitions between the conduction band and valence band. Taking into account the orthonormality of the bands, the derivative operator has to act on the lattice-periodic function $u_{\lambda,\mathbf{k}}$ to yield nonzero contributions. Explicitly, we have

$$h^{\mathrm{v,c}}_{\mathbf{k}',\mathbf{k}} = \frac{ie\hbar}{SM}\int d^2r A(\mathbf{r}) e^{i(\mathbf{k}-\mathbf{k}')\cdot\mathbf{r}} u^*_{\mathrm{v},\mathbf{k}'}(\mathbf{r})\mathbf{e}\cdot\nabla_{\mathbf{r}} u_{\mathrm{c},\mathbf{k}}(\mathbf{r}). \quad (2)$$

Here, S is the size of the system, given by the size of a unit cell, S_{cell}, times the number of sites in the system, N_{sites}.

At this stage, we make the following approximation (approximation 1): The vector potential, as well as the exponential in Eq. (2), vary on a length scale much larger than one unit cell. That is, we assume these quantities to be constant within a unit cell, but we keep variations beyond the scale of a unit cell. Hence this approximation is less restrictive than the usual dipole approximation which would fully ignore the spatial structure of the light. Yet without considering a particular choice of vector potential, the spatial variations of the beam are generally limited by a length scale on the order of the wavelength of the light. The same length scale also determines the variation of the exponential $e^{i(\mathbf{k}-\mathbf{k}')\cdot\mathbf{r}}$, since it will turn out *a posteriori* that $\mathbf{k}-\mathbf{k}'$ is determined through the photon momentum. Since the optical wavelength is usually several orders of magnitude larger than the size of the unit cell, the approximation is totally valid in the usual cases, but might not hold in some special cases, e.g., of Moiré lattices with enlarged unit cells [26–29]. Applying approximation 1 to Eq. (2), we write

$$\begin{aligned} h^{\mathrm{v,c}}_{\mathbf{k}',\mathbf{k}} &= \frac{ie\hbar}{MN_{\mathrm{sites}}}\sum_{\mathbf{R}_i} A(\mathbf{R}_i) e^{i(\mathbf{k}-\mathbf{k}')\cdot\mathbf{R}_i} \\ &\quad\times \frac{1}{S_{\mathrm{cell}}}\mathbf{e}\cdot\left[\int_{\mathrm{cell}} d^2r u^*_{\mathrm{v},\mathbf{k}'}(\mathbf{r})\nabla_{\mathbf{r}} u_{\mathrm{c},\mathbf{k}}(\mathbf{r})\right] \\ &\equiv (\hbar/M) A_{\boldsymbol{\kappa}} \times \mathbf{e}\cdot\mathbf{p}^{\mathrm{vc}}_{\mathbf{k}',\mathbf{k}}, \end{aligned} \quad (3)$$

where $\boldsymbol{\kappa} = \mathbf{k}-\mathbf{k}'$ and $A_{\boldsymbol{\kappa}} = \frac{1}{N_{\mathrm{sites}}}\sum_{\mathbf{R}_i} A(\mathbf{R}_i) e^{i\boldsymbol{\kappa}\cdot\mathbf{R}_i}$ is the Fourier transform of the vector potential. The dipole moment between the $\mathbf{k}'$ state in the valence band and the $\mathbf{k}$ state in the conduction band is denoted by $\mathbf{p}^{\mathrm{vc}}_{\mathbf{k}',\mathbf{k}}$.

We proceed by making a second approximation (approximation 2): The dipole moment depends only weakly on the wave vectors $\mathbf{k}$ and $\mathbf{k}'$. Indeed, the most radical implementation of this approximation in which the dipole moment is set to a constant $\mathbf{p}^{\mathrm{vc}}_0$ is commonly used in the literature; cf. Ref. [2]. To be less restrictive, we argue that $\mathbf{p}^{\mathrm{vc}}_{\mathbf{k}',\mathbf{k}}$ may depend on $\mathbf{k}+\mathbf{k}'$ (which can take relatively large values), whereas the dependence on $\mathbf{k}-\mathbf{k}'$ (which remains small since it is equivalent to the photon momentum) is negligible. To this end, we introduce the quantity $\mathbf{K} = \frac{1}{2}(\mathbf{k}+\mathbf{k}')$ and assume a linear (or linearized) dependence on $\mathbf{K}$:

$$\mathbf{p}^{\mathrm{vc}}_{\mathbf{K}} = \mathbf{p}^{\mathrm{vc}}_0 + (\boldsymbol{\alpha}\cdot\mathbf{K})\mathbf{p}^{\mathrm{vc}}_1. \quad (4)$$

For notational convenience, we write $\mathbf{e}\cdot\mathbf{p}^{\mathrm{vc}}_{\mathbf{K}} = p^{\mathrm{vc}}_{\mathbf{K}} = p^{\mathrm{vc}}_0 + (\boldsymbol{\alpha}\cdot\mathbf{K})p^{\mathrm{vc}}_1$. The light-matter matrix element is finally written as

$$h^{\mathrm{v,c}}_{\mathbf{k}',\mathbf{k}} = h^{\mathrm{vc}}_{\boldsymbol{\kappa},\mathbf{K}} = (\hbar/M) A_{\boldsymbol{\kappa}} p^{\mathrm{vc}}_{\mathbf{K}}. \quad (5)$$

This expression makes it immediately clear that the wave vector $\boldsymbol{\kappa}$ is exclusively selected by properties of the light field, whereas the wave vector $\mathbf{K}$ is exclusively determined by material properties. In the following, we will find that, in the case of exciton transitions, $\boldsymbol{\kappa}$ ($\mathbf{K}$) is related to the c.m. (relative) momentum of the exciton.

B. Exciton transitions

We are now interested in the transition amplitude for exciton formation $\mathcal{T}_X \equiv \langle X|H_{\rm LM}|{\rm vac}\rangle$. Here, $|X\rangle$ denotes an excitonic state, which in 2D is characterized through four quantum numbers for relative and c.m. motion. We choose $|X\rangle = |\mathbf{k}_{\rm c.m.}, n, j\rangle$, i.e., we describe the excitonic state by its linear c.m. momentum $\mathbf{k}_{\rm c.m.}$, and its hydrogenic quantum numbers n and j, representing the relative degrees of freedom. The vacuum state $|{\rm vac}\rangle$ corresponds to a filled valence band and an empty conduction band.

The excitonic wave function can be written as

$$\langle \mathbf{R}, \mathbf{r}|X\rangle \equiv \Phi^{\mathbf{k}_{\rm c.m.}}_{n,j}(\mathbf{R}, \mathbf{r}) \equiv \Phi^{\rm (c.m.)}_{\mathbf{k}_{\rm c.m.}}(\mathbf{R}) \times \Phi^{\rm (rel)}_{n,j}(\mathbf{r}), \quad (6)$$

where $\mathbf{r} = \mathbf{r}_{\rm e} - \mathbf{r}_h$ are relative coordinates of an electron-hole pair and $\mathbf{R} = \frac{1}{2}(\mathbf{r}_{\rm e} + \mathbf{r}_{\rm h})$ are the c.m. coordinates. The relative motion of electron and hole is described by the solutions to the 2D hydrogen atom, which are given by [2]

$$\Phi^{\rm (rel)}_{n,j}(\mathbf{r}) = \tilde{\mathcal{N}}_{n,j} f_{nj}(r) e^{ij\phi_r} = \tilde{\mathcal{N}}_{n,j} \rho^{|j|} e^{-\frac{|\rho|}{2}} L^{2|j|}_{n-|j|}(\rho) e^{ij\phi_r}, \quad (7)$$

where $\rho = r\rho_n$, with the inverse length scale given by $\rho_n = \frac{2}{(n+1/2)a_0}$. The material-specific length scale $a_0 = \hbar^2\epsilon/(e^2 M)$ is the effective Bohr radius depending on effective mass M and dielectric constant ϵ. The normalization of the relative wave function is given by

$$\tilde{\mathcal{N}}_{n,j} = \sqrt{\frac{(n-|j|)!}{(n+|j|)!}\left(\frac{\rho_n}{2}\right)^2 \frac{1}{\pi}\frac{1}{n+1/2}}. \quad (8)$$

For the c.m. part, we simply assume plane waves, $\Phi^{\rm (c.m.)}_{\mathbf{k}_{\rm c.m.}}(\mathbf{R}) = e^{i\mathbf{k}_{\rm c.m.}\cdot\mathbf{R}}$.

Without making use of the explicit solution for the excitonic wave functions, we write for the transition amplitude

$$\mathcal{T}_X = \int d^2\mathbf{R} \int d^2\mathbf{r} \sum_{\boldsymbol{\kappa},\mathbf{K}} \langle X|\mathbf{R}, \mathbf{r}\rangle \langle \mathbf{R}, \mathbf{r}|\boldsymbol{\kappa}, \mathbf{K}\rangle \times \langle \boldsymbol{\kappa}, \mathbf{K}|H_{\rm LM}|{\rm vac}\rangle. \quad (9)$$

The last term corresponds to the band-to-band transition amplitude evaluated above,

$$\langle \boldsymbol{\kappa}, \mathbf{K}|H_{\rm LM}|{\rm vac}\rangle = \left\langle \mathbf{K} - \frac{\boldsymbol{\kappa}}{2}|H_{\rm LM}|\mathbf{K} + \frac{\boldsymbol{\kappa}}{2}\right\rangle = h^{\rm v,c}_{\mathbf{K}-\frac{\boldsymbol{\kappa}}{2},\mathbf{K}+\frac{\boldsymbol{\kappa}}{2}} = (\hbar/M) A_{\boldsymbol{\kappa}} p^{\rm vc}_{\mathbf{K}}, \quad (10)$$

which is Fourier transformed to spatial coordinates by the second term,

$$\langle \mathbf{R}, \mathbf{r}|\boldsymbol{\kappa}, \mathbf{K}\rangle = \frac{1}{S^2} e^{i(\mathbf{K}+\frac{\boldsymbol{\kappa}}{2})\cdot\mathbf{r}_{\rm e} - i(\mathbf{K}-\frac{\boldsymbol{\kappa}}{2})\cdot\mathbf{r}_{\rm h}} = \frac{1}{S^2} e^{i(\mathbf{K}\cdot\mathbf{r} + i\boldsymbol{\kappa}\cdot\mathbf{R})}. \quad (11)$$

This expression explicitly shows that the wave vector $\boldsymbol{\kappa}$ ($\mathbf{K}$) is conjugate to the c.m. (relative) variable.

Plugging all expressions into Eq. (9), the $\mathbf{R}$ integral is immediately evaluated into a Kronecker delta $\delta_{\boldsymbol{\kappa},\mathbf{k}_{\rm c.m.}}$, so photon momentum $\boldsymbol{\kappa}$ and c.m. momentum $\mathbf{k}_{\rm c.m.}$ must match. We obtain

$$\mathcal{T}_X = \frac{\hbar(2\pi)^2 \tilde{\mathcal{N}}_{nj}}{MS^2} A_{\mathbf{k}_{\rm c.m.}} \int d^2\mathbf{r} f_{nj}(r) e^{ij\phi_r} \times \sum_{\mathbf{K}} e^{i\mathbf{K}\cdot\mathbf{r}} \left(p^{\rm vc}_0 + \boldsymbol{\alpha}\cdot\mathbf{K} p^{\rm vc}_1\right). \quad (12)$$

The $\mathbf{K}$ sum is a Fourier transform into the relative variable $\mathbf{r}$, and we can write $\sum_{\mathbf{K}} e^{i\mathbf{K}\cdot\mathbf{r}}(p^{\rm vc}_0 + \boldsymbol{\alpha}\cdot\mathbf{K}p^{\rm vc}_1) = (2\pi)^2[p^{\rm vc}_0\delta(\mathbf{r}) - ip^{\rm vc}_1 \boldsymbol{\alpha}\cdot\nabla_{\mathbf{r}}\delta(\mathbf{r})]$. From this expression it can immediately be seen that a constant dipole moment leads to nonzero transition amplitudes only if the relative exciton wave function $f_{nj}(r)$ is nonzero at $r = 0$. This is the case only for s excitons. The linear dependence of the dipole momentum on $\mathbf{K}$, expressed by the second term, gives rise to nonvanishing transition amplitudes if the first derivative of $f_{nj}(r)$ is nonzero at $r = 0$.

This second term enables the formation of excitons in higher-momentum states than the s series. However, we emphasize that this term is independent from the light source, and with respect to the relative degrees of freedom (n, j), we get the same transitions, no matter what the spatial structure of the light might be (as long as approximation 1 holds). Our analysis shows that the Elliott formula is unchanged by the spatial structure of light beyond the scale of the unit cell.

Our result agrees with a recent experiment in 2D transition metal dichalcogenides (TMDs) where twisted light has been used to reveal lightlike exciton dispersion [25]. Using nonresonant Laguerre-Gaussian beams, they observed a blueshift of the exciton energy that increased with ℓ; this indicates that the OAM was transferred preferentially to the c.m. of the exciton during its creation. However, we stress that our results apply much more generally since no particular 2D semiconductor or spatial light profile was specified during the analysis. This implies that the dispersion of all 2D excitons could be probed in a similar manner, presenting an alternative method to the traditional angle-resolved photoluminescence measurements [21].

We conclude this section by noting that, depending on material properties such as (i) the shape of carrier interactions or (ii) effective carrier masses, the excitonic wave function might be different from the one given above, without giving rise to modification of the selection rule: (i) The hydrogenic character of the relative wave function [Eq. (7)] is a consequence of Coulombic interactions between electron and hole, whereas screening effects in truly 2D materials typically modify the shape of the potential, e.g., giving rise to Rytova-Keldysh potentials [30]. However, since the selection rules obtained from Eq. (12) do not depend on the explicit form of the relative wave function, but only on its value at $r = 0$, our claim of vanishing $\mathcal{T}_X$ for all but s-type excitons still holds for this case. Notwithstanding, the numerical values of the nonzero $\mathcal{T}_X$ (see next section) can be affected by the shape of the potential. (ii) By identifying $\mathbf{R}$ with the c.m. position of the electron-hole pair, we have assumed equal effective masses for both carrier types. If this is not the case, the c.m. position is actually given by $\mathbf{R}^{\rm (c.m.)} = \mathbf{R} + \frac{m_{\rm e}-m_{\rm h}}{2(m_{\rm e}+m_{\rm h})}\mathbf{r} \equiv \mathbf{R} + \delta_m\mathbf{r}$. Hence the excitonic c.m. wave function will be modified to $\Phi^{\rm (c.m.)}_{\mathbf{k}_{\rm c.m.}}(\mathbf{R}^{\rm (c.m.)}) = e^{i\mathbf{k}_{\rm c.m.}\cdot(\mathbf{R}+\delta_m\mathbf{r})}$. In Eq. (12), the additional term $e^{i\delta_m\mathbf{k}_{\rm c.m.}\cdot\mathbf{r}}$ will not modify the sum in $\mathbf{K}$; hence (for $\boldsymbol{\alpha} = 0$) nonzero $\mathcal{T}_X$ still requires a nonzero exciton wave function at $r = 0$. Thus the selection rule also holds in the case of unequal effective masses.

III. EXAMPLE: EXCITONS FROM TWISTED LIGHT

Thus far, we have been very general in our treatment with respect to the profile of the optical excitation. In the following,

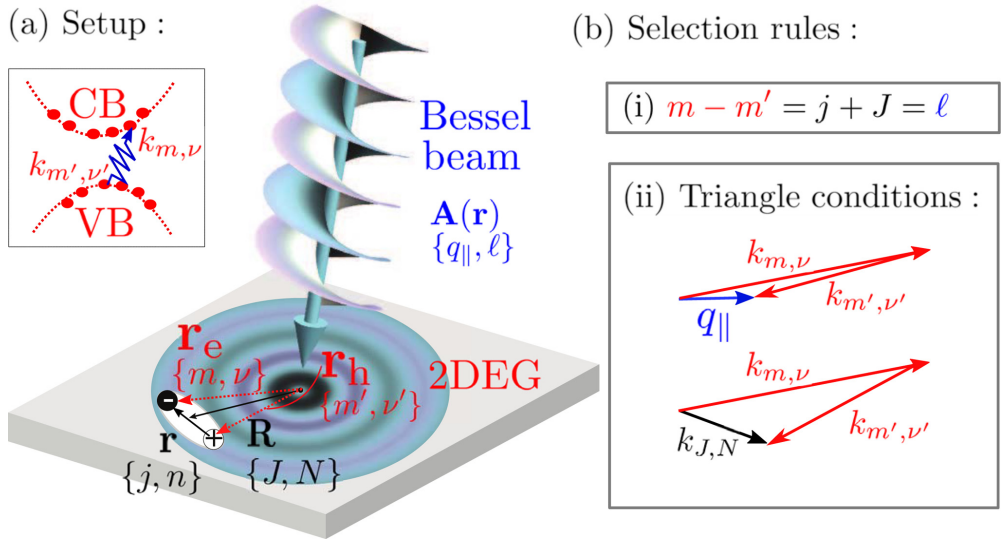

FIG. 1. (a) A Bessel light beam **A** with photon momentum or angular momentum $(q_\parallel, \ell)$ creates an electron-hole pair in a 2D electron gas (2DEG). The electron (hole) is characterized by quantum numbers (m, ν) $[(m', \nu')]$ for angular momentum or momentum. The pair can form a bound state, and the degrees of freedom of such an exciton are the center-of-mass motion, characterized by angular momentum or momentum quantum numbers (J, N), and the relative motion, characterized by quantum numbers (j, n) for angular momentum and energy. CB, conduction band; VB, valence band. (b) The selection rules for optical transitions and exciton formation reflect (i) conservation of angular momentum and (ii) conservation of linear momentum, reflected by the illustrated triangle conditions.

we are going to treat the specific case of a Bessel beam and, besides the analytical treatment along the lines presented in the previous sections, we will also present the result of numerical evaluations. With this choice of the vector potential, our system exhibits a cylindrical symmetry, since the light field has an azimuthal phase dependence $\exp(i\ell\phi)$, where ℓ defines the OAM per photon (in units of $\hbar$). To match this symmetry, we consider a cylindrical sample, noting that the sample geometry becomes irrelevant in the thermodynamic limit. Accordingly, we adapt our theoretical description to this symmetry and express the light-matter coupling in terms of a cylindrical wave function; see also Refs. [23,24]. We illustrate this case in Fig. 1, where we also sketch the resulting selection rules in terms of the good quantum numbers for the cylindrical symmetry.

A. Band-to-band transitions in the cylindrical basis

Instead of plane waves with linear momentum quantum number, the electronic basis in a cylindrical sample is best described by wave functions $\varphi_{m,\nu}(\mathbf{r}) = \mathcal{N}_{m,\nu} J_m(k_{m,\nu} r)\exp(im\phi)$, which solve the Schrödinger equation for free electrons with cylindrical boundary conditions. Here, $J_m(x)$ denotes the mth Bessel function, and the momenta $k_{m,\nu}$ must be chosen such that the wave function vanishes at the system boundary (i.e., for $|\mathbf{r}| = R_0$). Therefore we have $k_{m,\nu} = x_{m,\nu}/R_0$, with $x_{m,\nu}$ being the νth zero of the mth Bessel function. The normalization is given by $\mathcal{N}_{m,\nu} = (R_0\sqrt{\pi}|J_{|m-1|}(x_{m,\nu})|)^{-1}$. As in the previous section, the crystal lattice is taken into account by multiplying the wave functions $\varphi_{m,\nu}$ with lattice-periodic Bloch functions $u_\lambda(\mathbf{r})$ for the bands λ. For simplicity, the Bloch functions are assumed to be independent from the quantum numbers m and ν. With this, the electronic basis is given:

$$\varphi_{\lambda;m,\nu}(\mathbf{r}) = \mathcal{N}_{m,\nu} J_m(k_{m,\nu} r)\exp(im\phi) u_\lambda(\mathbf{r}). \tag{13}$$

In this basis, the light-matter transition amplitudes in the Coulomb gauge (within the weak-field limit) are given by

$$h^{\mathrm{v,c}}_{m,\nu;m',\nu'} = \frac{-i\hbar e}{SM}\int d\mathbf{r}\bar{\varphi}_{+,m',\nu'}(\mathbf{r})[\mathbf{A}(\mathbf{r})\cdot\nabla_{\mathbf{r}}]\varphi_{-,m,\nu}(\mathbf{r}), \tag{14}$$

with $\bar{\varphi}$ denoting the complex conjugate of φ.

Before we proceed, let us first fix the vector potential. We consider a vector potential which in the sample plane reads $\mathbf{A}(\mathbf{R}) = A_0 a(R) e^{i\ell\phi}\mathbf{e}_\sigma$, where $\mathbf{e}_\sigma$ is the polarization in the plane. For a circularly polarized Bessel beam with OAM ℓ, we have $a(R) = J_\ell(q_\parallel R)$, with $q_\parallel$ being the in-plane photon momentum. Note that a vertical contribution to the vector potential, needed to fulfill Maxwell's equation, is neglected here since it is not relevant for light-matter interaction with a two-dimensional medium. However, it is important to keep in mind that the frequency ω of the photon depends also on the perpendicular momentum component q_z, $\omega = \frac{c}{\hbar}\sqrt{q_\parallel^2 + q_z^2}$.

Invoking approximations 1 and 2, both $\mathbf{A}(\mathbf{r})$ and $J_m(k_{m,\nu} r)\exp(im\phi)$ can be considered constant on the scale of the lattice constant a. Thus the evaluation of $h^{\mathrm{v,c}}_{m,\nu;m',\nu'}$ can be split into an integral $\mathcal{I}$ restricted to the unit cell and a sum over unit cells $\mathcal{S}_{m,\nu;m',\nu'}$; that is, we can write $h^{\mathrm{v,c}}_{m,\nu;m',\nu'} = \frac{-i\hbar}{SM}\mathcal{S}_{m,\nu;m',\nu'} \times \mathcal{I}$. As before, the sum over the whole system takes into account the variation of the light field, occurring on larger scales, whereas the unit cell integral determines the material's dipole moment taken to be a constant.

Explicitly, the two contributions are given by

$$\mathcal{I} = e\int_{\mathrm{c}} d\mathbf{r}\bar{u}_+(\mathbf{r})(\mathbf{e}_\sigma\cdot\nabla_{\mathbf{r}})u_-(\mathbf{r}) \tag{15}$$

and

$$\mathcal{S}_{m,\nu;m',\nu'} = \mathcal{N}_{m,\nu}\mathcal{N}_{m',\nu'}A_0 \sum_i J_m(k_{m,\nu}R_i)J_{m'}(k_{m',\nu'}R_i) \times J_\ell(q_\parallel R_i)\exp[i(m-m'+\ell)\phi_i], \tag{16}$$

where (R_i, ϕ_i) denote the lattice vectors. In analogy to Eq. (3), we can read off the results of the cell integral $\mathcal{I}$ as the interband dipole moment $p_{\mathrm{vc}} \equiv \mathbf{e}_\sigma \cdot \mathbf{d} = \mathcal{I}$, which depends only on the material. Since we take it to be constant here, it will enter the transition amplitudes only as a prefactor. To evaluate $\mathcal{S}_{m,\nu;m',\nu'}$, we replace the summation over cells by an integral. With this, we immediately arrive at a first selection rule from the angular part of the integral:

$$\mathcal{S}_{m,\nu;m',\nu'} \propto \delta_{\ell+m-m'}. \tag{17}$$

The radial integral in $\mathcal{S}_{m,\nu;m',\nu'}$ is over a product of three Bessel functions, $\mathcal{S}_{m,\nu;m',\nu'} \propto \int_0^{R_0} dr\, rJ_m(k_{m,\nu}r)J'_m(k_{m',\nu'}r)J_\ell(q_\parallel r)$. Its analytic solution (in the limit $R_0 \to \infty$) has been derived in Ref. [31] and can also be found in Appendix A. Here, we only consider that, from this solution, the integral takes nonzero values only if a triangle condition is fulfilled: The three scalars $k_{m,\nu}$, $k_{m',\nu'}$, and $q_\parallel$ must be such that they can form a triangle (including the limit in which the triangle is squeezed into a line). Therefore this condition yields a second selection rule: The change in electron momentum upon a band-to-band transition is bounded by the in-plane momentum of the photon.

B. Exciton transitions

The amplitudes $h^{\mathrm{v,c}}_{m,\nu;m',\nu'}$ quantify the band-to-band transition which generates an electron-hole pair characterized by $m - m' = \ell$ and $|k_{m,\nu} - k_{m',\nu'}| \leqslant q_\parallel$. Next, we have to ask which excitonic states can be formed from these pairs. In accordance with the presumed cylindrical symmetry of the system, we now also describe the excitonic states in terms of cylindrical-symmetric quantum numbers, $|X\rangle = |N, J, n, j\rangle$, where n, j account for the state of relative motion (as before) and N, J account for the c.m. degrees of freedom (instead of $\mathbf{k}_{\mathrm{c.m.}}$ used in the previous section). Again, the excitonic wave function is a product of the relative ($\mathbf{r}$) and c.m. ($\mathbf{R}$) contributions: $\langle \mathbf{R}, \mathbf{r}|X\rangle \equiv \Phi^{J,N}_{n,j}(\mathbf{R}, \mathbf{r}) \equiv \Phi^{(\mathrm{c.m.})}_{N,J}(\mathbf{R}) \times \Phi^{(\mathrm{rel})}_{n,j}(\mathbf{r})$. The relative part is unchanged, given by Eq. (7). Since the c.m. of the exciton is subject to the same boundary conditions as the electron and hole individually, its wave function is given by

$$\Phi^{(\mathrm{c.m.})}_{J,N}(\mathbf{R}) = \mathcal{N}_{J,N}J_J(k_{J,N}R)\exp(iJ\phi_{\mathrm{c.m.}}), \tag{18}$$

where the quantum number J denotes the angular momentum of the c.m. and both J and N together define the total c.m. momentum $Q_{\mathrm{c.m.}} = x_{J,N}/R_0$.

Projecting the excitonic wave function onto the rotationally symmetric basis for electron and hole wave functions is equivalent to a Hankel transform. This projection yields a quantity $\mathcal{B}^{n,j;J,N}_{m,\nu;m',\nu'}$:

$$\mathcal{B}^{n,j;J,N}_{m,\nu;m',\nu'} = \mathcal{N}_{m,\nu}\mathcal{N}_{m',\nu'} \int d\mathbf{r}_{\mathrm{e}} \int d\mathbf{r}_{\mathrm{h}} \bar{\Phi}^{J,N}_{n,j}(\mathbf{R}, \mathbf{r}) \times J_m(k_{m,\nu}r_{\mathrm{e}})J_{m'}(k_{m',\nu'}r_{\mathrm{h}})\exp[i(m\phi_{\mathrm{e}} - m'\phi_{\mathrm{h}})]. \tag{19}$$

An explicit analytic expression which solves this integral is provided in Appendix B. As before for $\mathcal{S}_{m,\nu;m',\nu'}$, we also encounter a triangle condition in the evaluation of $\mathcal{B}^{n,j;J,N}_{m,\nu;m',\nu'}$: It is nonzero only if the lengths $k_{m,\nu}$, $k_{m',\nu'}$, and $k_{J,N}$ form a triangle, i.e., $|k_{m,\nu} - k_{m',\nu'}| \leqslant k_{J,N}$. More importantly, as shown in Appendix B, one of the integrals in Eq. (19) yields a Kronecker δ:

$$\mathcal{B}^{n,j;J,N}_{m,\nu;m'\nu'} \sim \delta_{j+J,m-m'}. \tag{20}$$

Together with the selection rule for band-to-band transitions [Eq. (17)], Eq. (20) reflects conservation of angular momentum.

We are now in a position to calculate the exciton transition amplitude $\mathcal{T}^{J,N}_{n,j} \equiv \langle X^{J,N}_{n,l}|H_{\mathrm{LM}}|\mathrm{vac}\rangle$:

$$\mathcal{T}^{J,N}_{n,j} = \sum_{m,\nu;m',\nu'} h^{\mathrm{v,c}}_{m,\nu;m',\nu'}\mathcal{B}^{n,j;J,N}_{m,\nu;m'\nu'}. \tag{21}$$

These sums should go over all occupied (empty) levels m', ν' (m, ν), but a more practical limitation of these sums is due to the fact that $\mathcal{B}^{n,j;J,N}_{m,\nu;m'\nu'} \approx 0$ when either $k_{m,\nu}$ or $k_{m',\nu'}$ become much larger than the inverse of the Bohr radius, a_0^{-1}.

C. Numerical evaluation

The last observation allows us to introduce a cutoff momentum $k_{\mathrm{cut}} \gg a_0^{-1}$ at which the sums can be truncated. With this, the numerical evaluation of Eq. (21) become feasible. For concreteness, by comparison of $\mathcal{T}^{J,N}_{n,j}$ obtained from different cutoff momenta k_{cut}, we estimate that the relative error remains below 0.1 for $k_{\mathrm{cut}}a_0 \geqslant 3.75$. In the numerical evaluation of $\mathcal{T}^{J,N}_{n,j}$ presented below, we have included 47 100 Bessel functions. With that, $k_{\mathrm{cut}}a_0 > 3.75$ for system sizes up to $R_0/a_0 = 12\,500$. We note that k_{cut} also restricts the sums in m and ν in the following way: $|m| < \pi k_{\mathrm{cut}}R$ and/or $\nu < k_{\mathrm{cut}}R$.

The numerical evaluation confirms the analytical result from Sec. II that the Elliott formula remains unchanged by the spatial structure of the light source. To this end, we obtained the height of the spectral lines, $\tilde{\mathcal{T}}_{n,j}$, by summing the contributions from all c.m. momentum modes at a given n and j:

$$\tilde{\mathcal{T}}_{n,j} = \frac{1}{\mathcal{N}_{\mathcal{T}}} \sum_{N,J} \mathcal{T}^{J,N}_{n,j}. \tag{22}$$

To make this quantity independent from the intensity of the light, we normalize by $\mathcal{N}_{\mathcal{T}} = \sqrt{\sum_{n,j,N} |\mathcal{T}^{J,N}_{n,j}|^2}$. The results are shown in Table I for a system of size $R_0 = 10^4 a_0$ in a Bessel beam with OAM $\ell = 0$ and $\ell = 1$ and in-plane photon momentum $q_\parallel = 10^{-3}a_0^{-1}$. For comparison, we also provide the results from the 2D Elliott formula for an infinite system. All values agree very well with each other.

Our numerical evaluation also confirms the selection rule that the c.m. momentum of the exciton is determined by the linear in-plane momentum of the photon. To this end, we focus on the $1s$ transition and evaluate the strengths, $\mathcal{T}^{\ell,N}_{0,0}$, of transitions into the different c.m. modes $k_{\ell,N}$. The results, normalized by the peak value $\max_N(\mathcal{T}^{\ell,N}_{0,0})$, are shown in Fig. 2 for different values of photon OAM ℓ and photon momentum. The transition strength is clearly peaked for the c.m. momenta

TABLE I. Relative transition strength $|\tilde{\mathcal{T}}_{n,j}|^2$ for a system of size $R_0 = 10^4 a_0$ in a Bessel beam with OAM $\ell = 0$ and $\ell = 1$ and in-plane photon momentum $q_\parallel = 10^{-3} a_0^{-1}$. For comparison, we also provide the results from the 2D Elliott formula for an infinite system in a Gaussian beam.

	$1s$	$2s$	$3s$
OAM 0	0.998	0.037	0.0079
OAM 1	0.995	0.037	0.0079
2D Elliott	0.9993	0.037	0.0080

which match with the momentum of the photon, but barely depends on the OAM.

As a side note, we mention that, despite the relatively large size of the numerical basis and, correspondingly, of the cutoff momentum k_{cut}, our numerical procedure has not been able to verify the vanishing of transition matrix elements for $|j| > 0$. In fact for both cases, Gaussian beams with OAM $\ell = 0$ and twisted beams with OAM $\ell = 1$, the obtained numerical values for the transition matrix elements into p states take small but finite values. The reason for this discrepancy between analytical expectation and numerical results can be explained in the following way: while the relative wave function for s excitons is real, the wave functions for all other excitonic states carry a phase dependence $e^{ij\phi_r}$, which is responsible for the destructive interference, rendering these states optically dark. Therefore, although our numerical precision is sufficient to faithfully reproduce the analytical results for transitions into s states, for the other transition matrix elements the numerical errors are too large to clearly demonstrate their vanishing. A clear hint for interpreting these values as numerical artifacts is the observation that, by varying the system size and/or the photon momentum, the numeric values obtained for p transitions show, in contrast to the values for the s transitions, a strong nonmonotonic behavior. This observation points towards a numerical challenge if, for instance, under relaxation of approximation 2, the possibly nonzero values of p-transition elements shall be evaluated numerically.

Let us finally discuss the different length scales which appear in the calculation, that is, the effective Bohr radius a_0, the sample size R_0, and the inverse of the photon momentum $q_\parallel^{-1}$. In the calculation, we have taken the effective Bohr radius a_0 as the unit of length. With typical values of the dielectric constant being much greater than 1 (e.g., ≈ 13 in GaAs [32] and 7 in semiconducting TMDs [33]), and the effective mass being much smaller than the electron mass (e.g., 0.067 and 0.39 electron masses for the conduction band in GaAs [34] and model TMDs [35], respectively), the effective Bohr radius can significantly exceed the Bohr radius of the hydrogen atom (≈ 0.05 nm). Typical values range between 0.1 and 1 nm. Taking the numerical constraints into account (i.e., truncation errors), our study examines sample sizes R_0 on the order of 10^4 effective Bohr radii, which corresponds to sample sizes on the order of 1–10 μm. Importantly, this size is significantly larger than the optical vortex. Regarding the in-plane photon momentum $q_\parallel$, an upper limit is given by the inverse of the wavelength, $2\pi/\lambda_0$, assuming vertical incidence on the sample. The wavelength λ_0 is determined by the band gap of the material. As an estimate for this limit, we obtain 100 nm^{-1}. Thus our choice of $q_\parallel = 10^{-3} a_0^{-1}$ corresponds to the upper limit if $a_0 = 0.1$ nm, while this choice remains below that limit if a_0 is larger.

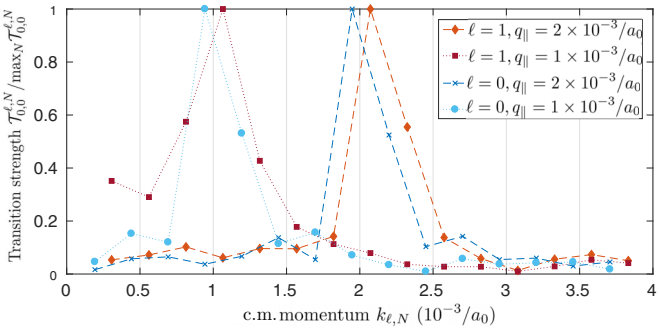

FIG. 2. For the $1s$ transition, we plot the transition strength $\mathcal{T}^{\ell,N}_{0,0}$ into the different c.m. modes $k_{\ell,N}$, normalized by the peak value $\max_N(\mathcal{T}^{\ell,N}_{0,0})$, for illumination with $\ell = 0$ and $\ell = 1$ Bessel beams. The peak is obtained for the best match between c.m. momentum $k_{\ell,N}$ and in-plane photon momentum, $q_\parallel = 10^{-3} a_0^{-1}$.

IV. SUMMARY AND CONCLUSIONS

We have shown that the vector potential selects the c.m. quantum numbers (absolute value of c.m. momentum + c.m. angular momentum) but has no effect on the amplitudes of transitions into states with different relative quantum numbers n and j. This implies that Elliott's formula is unchanged by the structure in the light field. The approximation which gives rise to this conclusion is the separation of length scales: unit cell vs wavelength. This assumption implies that $A(x)$ and e^{iqx} are constant on the the level of a unit cell, and for the dipole moment, $p^{\text{vc}}_{\mathbf{k},\mathbf{k}+\mathbf{q}} \approx p^{\text{vc}}_{\mathbf{k},\mathbf{k}}$. We have confirmed our general analytical result by performing numerical evaluations for the concrete case of Bessel beams in a circularly symmetric sample. Qualitatively, we have shown that, for a transition to be optically bright, the sum of both relative and c.m. angular momenta, $j + J$, must be equal to the OAM value ℓ of the light. Quantitatively, we have evaluated that the transition amplitudes are given by the Elliott formula.

While our results rule out twisted light for the generation of dark excitons, the predicted transfer of OAM to the c.m. degree of freedom can be useful from the perspective of quantum simulation, and especially from the point of view of artificial gauge fields. In Ref. [36], it has been shown that artificial flux is generated in a photonic system when OAM light is injected into a waveguide lattice. Excitons in tunable lattices have recently been shown to form strongly correlated many-body phases, such as Mott insulating phases [37] or checkerboard phases [38]. If, in the future, twisted light provided excitonic lattices with artificial magnetic fluxes, this could give rise to chiral Mott insulators [39] or extended supersolid regimes [40].

ACKNOWLEDGMENTS

We thank Bin Cao, Valentin Kasper, Maciej Lewenstein, Andrey Grankin, Sunil Mittal, Jay Sau, Deric Session, Glenn

Solomon, Daniel Suarez, and Jon Vanucci for thoughtful comments and fruitful discussions. T.G. and U.B. acknowledge funding from La Caixa Foundation (ID 100010434, Fellowship Code No. LCF/BQ/PI19/11690013), the European Research Council for ERC Advanced Grant NOQIA; Agencia Estatal de Investigación (R&D Project No. CEX2019-000910-S, funded by MCIN/AEI/10.13039/501100011033, Plan National FIDEUA PID2019-106901GB-I00, FPI, QUANTERA MAQS PCI2019-111828-2, Proyectos de I+D+I Retos Colaboración RTC2019-007196-7); Fundació Cellex; Fundació Mir-Puig; Generalitat de Catalunya through the CERCA program, AGAUR Grant No. 2017 SGR 134, QuantumCAT U16-011424, cofunded by ERDF Operational Program of Catalonia 2014-2020; EU Horizon 2020 FET-OPEN OPTOLogic (Grant No. 899794); National Science Centre, Poland (Symfonia Grant No. 2016/20/W/ST4/00314); Marie Skłodowska-Curie STREDCH Grant No. 101029393; La Caixa Junior Leaders fellowships (ID 100010434) and EU Horizon 2020 under Marie Skłodowska-Curie Grant Agreement No. 847648 (LCF/BQ/PI20/11760031, LCF/BQ/PR20/11770012, LCF/BQ/PR21/11840013). J.S. acknowledges support from the NSF Graduate Research Fellowship Program (GRFP) and the ARCS Foundation. J.S. and M.H. were supported by Grants No. AFOSR FA95502010223 and No. NSF PHY1820938 and by Grants No. NSF DMR-2019444, No. ARL W911NF1920181, and No. ARO W911NF2010232, the Simons Foundation, and the Minta Martin Foundation, respectively.

APPENDIX A: BAND-TO-BAND TRANSITION MATRIX FOR A BESSEL BEAM

The band wave functions are expressed in terms of Bessel functions $J_m(k_{m,\nu}r)$, and the spatial profile of the light is given by a Bessel beam $J_\ell(q_\parallel r)$. Thus the matrix elements for band-to-band transitions are proportional to the integral over a product of three Bessel functions:

$$\mathcal{S}_{m,\nu;m',\nu'} \propto \int_0^{R_0} dr\, r J_m(k_{m,\nu}r) J'_m(k_{m',\nu'}r) J_\ell(q_\parallel r). \tag{A1}$$

To evaluate this integral, we take the limit $R_0 \to \infty$ and follow the procedure as described in Ref. [31]; that is, we perform a plane-wave expansion of the Bessel functions. With this, the integral is found to take the following value:

$$\begin{aligned}\mathcal{J} &\equiv \int_0^\infty dr\, r J_m(k_{m,\nu}r) J'_m(k_{m',\nu'}r) J_\ell(q_\parallel r) \\ &= \begin{cases} \frac{1}{2\pi A_\triangle} \cos\left(m\alpha_2 - m'\alpha_1\right) & \text{if } k_{m,\nu}, k_{m',\nu'}, q_\parallel \text{can form a triangle,} \\ 0 & \text{otherwise.} \end{cases}\end{aligned} \tag{A2}$$

If a triangle with lengths $k_{m,\nu}$, $k_{m',\nu'}$, and $q_\parallel$ can be formed, the quantity $A_\triangle$ denotes the area of this triangle, and α_1 and α_2 are exterior angles of this triangle. Defining $\kappa \equiv (k_1 + k_2 + k_3)/2$, we have

$$A_\triangle = \sqrt{\kappa(\kappa - k_1)(\kappa - k_2)(\kappa - k_3)}. \tag{A3}$$

The angles are given by

$$\alpha_1 = \arccos\left(\frac{k_1^2 - k_2^2 - k_3^2}{2k_2k_3}\right), \tag{A4}$$

$$\alpha_2 = \arccos\left(\frac{k_2^2 - k_3^2 - k_1^2}{2k_1k_3}\right). \tag{A5}$$

APPENDIX B: HANKEL TRANSFORM OF THE EXCITON

In a circularly symmetric system, the electronic bands are conveniently given by Bessel functions. Decomposing the excitonic wave function in terms of these single-particle states is equivalent to a Hankel transform of the exciton. Let the relative motion of electron and hole of the exciton be described by a principal quantum number n and an angular momentum quantum number j, and the center-of-mass (c.m.) motion be described by quantum numbers J for angular momentum and momentum and N for momentum or energy. The overlap of such an exciton with an electron in a state described by quantum numbers m, ν and a hole described by m', ν' reads

$$\begin{aligned}\mathcal{B}^{n,j;J,N}_{m,\nu;m',\nu'} = \mathcal{N}_{m,\nu}\mathcal{N}_{m',\nu'} \int d\mathbf{r}_\mathrm{e} \int d\mathbf{r}_\mathrm{h} \bar{\Phi}^{(\mathrm{c.m.})}_{J,N}(\mathbf{R}) \bar{\Phi}^{(\mathrm{rel})}_{n,j}(\mathbf{r}) \\ \times J_m(k_{m,\nu}r_\mathrm{e}) J_{m'}(k_{m',\nu'}r_\mathrm{h}) \exp\left[i(m\phi_\mathrm{e} - m'\phi_\mathrm{h})\right].\end{aligned} \tag{B1}$$

Here, $\mathbf{R} = (\mathbf{r}_\mathrm{e} + \mathbf{r}_\mathrm{h})/2$ describes the c.m. motion, $\mathbf{r} = \mathbf{r}_\mathrm{e} - \mathbf{r}_\mathrm{h}$ describes the relative motion, and $\mathbf{r}_{\mathrm{e,h}}$ are expressed in polar coordinates $(r_{\mathrm{e,h}}, \phi_{\mathrm{e,h}})$. As a first step to evaluate $\mathcal{B}$, we will expand the Bessel functions (including the one contained in the definition of $\bar{\Phi}^{(\mathrm{c.m.})}_{J,N}$; see main text) in terms of plane waves. To this end, we note that

$$e^{iz\cos(\theta)} = \sum_{n=-\infty}^{n=\infty} i^n e^{in\theta} J_n(z). \tag{B2}$$

Therefore

$$e^{i\vec{k}\cdot\vec{r}_e} = e^{ikr_e\cos(\phi_e - \phi_k)} = \sum_{n=-\infty}^{n=\infty} i^n e^{in\phi_e} e^{-in\phi_k} J_n(kr_e). \tag{B3}$$

Integrating both sides over $\int_0^{2\pi} d\phi_k\, e^{im\phi_k}$ gives

$$J_m(kr_e)e^{im\phi_e} = \frac{1}{2\pi}(-i)^m \int_0^{2\pi} e^{i\vec{k}\cdot\vec{r}_e} e^{im\phi_k} d\phi_k. \tag{B4}$$

Applying this expansion, below we associate $\mathbf{k} \equiv (k, \phi_k)$ with electron momentum and $\mathbf{k}' \equiv (k', \phi_{k'})$ with hole momentum, where k and k' are introduced as shorthand notations for $k_{m,\nu}$ and $k_{m;,\nu'}$. Similarly, the center-of-mass momentum will be associated with a vector $\mathbf{Q} = Q, \phi_Q$. With this, and reexpressing electron and hole coordinates in terms of relative and

center-of-mass coordinates, we get

$$\mathcal{B}^{n,j;J,N}_{m,\nu;m',\nu'} = \tilde{\mathcal{N}}_{n,j}\mathcal{N}_{J,N}\mathcal{N}_{m,\nu}\mathcal{N}_{m',\nu'}\frac{-i^{m-m'+J}}{(2\pi)^3}\int_0^{2\pi}d\phi_k\int_0^{2\pi}d\phi_{k'}\int_0^{2\pi}d\phi_Q\int d\mathbf{r}\int d\mathbf{R}e^{i\mathbf{R}\cdot(\mathbf{k}-\mathbf{k}'-\mathbf{Q})}$$
$$\times e^{i\mathbf{r}\cdot(\mathbf{k}+\mathbf{k}')/2}e^{im\phi_k}e^{-im'\phi_{k'}}e^{-iJ\phi_Q}\rho^{|j|}e^{-\frac{|\rho|}{2}}L^{2|j|}_{n-|j|}(\rho)e^{-ij\phi_{\mathrm{rel}}}, \tag{B5}$$

where $\rho \equiv r\rho_n$ with $\rho_n \equiv 2r/[a_0(n+\frac{1}{2})]$. The integration in $\mathbf{R}$ yields a δ function, which imposes a triangle condition for the momenta:

$$\int d\mathbf{R}e^{i\mathbf{R}\cdot(\mathbf{k}-\mathbf{k}'-\mathbf{Q})} = (2\pi)^2\delta^{(2)}(\mathbf{k}-\mathbf{k}'-\mathbf{Q}). \tag{B6}$$

Let us next carry out the angular part of the integral in $\mathbf{r}$:

$$\int d\phi_{\mathrm{rel}}e^{-ij\phi_{\mathrm{rel}}}e^{irq\cos(\phi_{\mathrm{rel}}-\phi_q)} = 2\pi i^j e^{-ij\phi_q}J_j(qr). \tag{B7}$$

Here, as a shorthand notation, we have introduced $\mathbf{q} = (q,\phi_q) \equiv \frac{\mathbf{k}+\mathbf{k}'}{2}$. For the radial part of the relative position integral we write

$$f(q,n,j) \equiv \int d\rho\rho^{j+1}e^{-\frac{\rho}{2}}L^{2j}_{n-j}(\rho)J_j\left(\frac{q}{\rho_n}\rho\right) = \sum_{s=0}^{n-j}\frac{\sqrt{2}(-1)^s(\frac{q}{\rho_n})^j}{\left(\frac{2q^2}{\rho_n^2}+\frac{1}{2}\right)^{j+s+\frac{3}{2}}}\frac{\Gamma(n+j+1)\Gamma(2j+s+2)}{\Gamma(s+1)\Gamma(j+1)\Gamma(n-j-s+1)\Gamma(2j+s+1)}$$
$$\times\ {}_2F_1\left(\frac{-s}{2},\frac{-1-s}{2},1+j,-\frac{4q^2}{\rho_n^2}\right), \tag{B8}$$

with ${}_2F_1$ being the hypergeometric function. Note that here we have changed the integration variable from r to ρ, which yields a factor $1/\rho_n^2$. For the analytic solution of the integral, we have taken the integration boundary to be at infinity.

Putting all together, we arrive at the following intermediate result:

$$\mathcal{B}^{n,j;J,N}_{m,\nu;m',\nu'} = \tilde{\mathcal{N}}_{n,j}\mathcal{N}_{J,N}\mathcal{N}_{m,\nu}\mathcal{N}_{m',\nu'}\frac{i^{m-m'+J+j}}{\rho_n^2}f(q,n,j)$$
$$\times\int_0^{2\pi}d\phi_k\int_0^{2\pi}d\phi_{k'}\int_0^{2\pi}d\phi_Q\delta^{(2)}(\mathbf{k}-\mathbf{k}'-\mathbf{Q})e^{i(m\phi_k-m'\phi_{k'}-j\phi_q-J\phi_Q)}. \tag{B9}$$

Let us for a moment assume ϕ_Q to be fixed. Then, in the remaining two integrals, ϕ_k and $\phi_{k'}$ will be fixed such that the triangle condition expressed by the δ function is met. To proceed, we write the delta function $\delta^{(2)}(\vec{k}-\vec{k}'-\vec{Q})$ explicitly in terms of ϕ_k, $\phi_{k'}$, and ϕ_Q:

$$\delta^{(2)}\left(\vec{k}-\vec{k}'-\vec{Q}\right) = \delta(k\cos\phi_k - k'\cos\phi_{k'} - Q\cos\phi_Q)\delta(k\sin\phi_k - k'\sin\phi_{k'} - Q\sin\phi_Q). \tag{B10}$$

To perform the integral over these δ functions, we first note the identity

$$\int d\phi g(\phi)\delta[h(\phi)] = \sum_w \left.\frac{g(\phi^w)}{\left|\frac{dh(\phi)}{\phi}\right|}\right|_{\phi=\phi^w}, \tag{B11}$$

where $\phi = \phi^w$ denote the solutions to $h(\phi) = 0$. We define $h_1(\phi_k) = k\cos\phi_k - k'\cos\phi_{k'} - Q\cos\phi_Q$ and $h_2(\phi_{k'}) = k\sin\phi_k - k'\sin\phi_{k'} - Q\sin\phi_Q$. The zeros of h_1 and h_2 are given by

$$\cos\phi_k = \frac{k'\cos\phi_{k'} + Q\cos\phi_Q}{k}, \tag{B12}$$

$$\sin\phi_{k'} = \frac{k\sin\phi_k - Q\sin\phi_Q}{k'}. \tag{B13}$$

If there is a triangle with lengths given by k, k', and Q, the angles ϕ_k and $\phi_{k'}$ of such triangle solve these equations. Note that a second solution can then be obtained from a mirror transformation of the triangle, but since the solutions are equivalent, considering only one of them is sufficient. On the other hand, if such triangle does not exist, Eq. (B12) has no solution, and the integral is zero. Explicitly, the solutions can be written as

$$\phi_k = \tilde{\phi}_k + \phi_Q \quad \text{with } \tilde{\phi}_k = \arccos\left(\frac{k^2+Q^2-k'^2}{2kQ}\right), \tag{B14}$$

$$\phi_{k'} = \tilde{\phi}_{k'} + \phi_Q \quad \text{with } \tilde{\phi}_{k'} = \arccos\left(\frac{k^2-Q^2-k'^2}{2k'Q}\right). \tag{B15}$$

The angle ϕ_q in Eq. (B9) is given by

$$\phi_q = \tan^{-1}\left(\frac{q_y}{q_x}\right) = \tan^{-1}\left(\frac{k_y + k'_y}{k_x + k'_x}\right) = \tan^{-1}\left(\frac{k\sin(\tilde{\phi}_k - \phi_Q) + k'\sin(\tilde{\phi}_{k'} - \phi_Q)}{k\cos(\tilde{\phi}_k - \phi_Q) + k'\cos(\tilde{\phi}_{k'} - \phi_Q)}\right)$$
$$= \tan^{-1}\left(\frac{k\sin(\tilde{\phi}_k) + k'\sin(\tilde{\phi}_{k'})}{k\cos(\tilde{\phi}_k) + k'\cos(\tilde{\phi}_{k'})}\right) + \phi_Q \equiv \tilde{\phi}_q + \phi_Q. \tag{B16}$$

We can also express q in terms of k, k', $\tilde{\phi}_k$, and $\tilde{\phi}_{k'}$:

$$q = \frac{1}{2}\sqrt{k^2 + k'^2 + kk'\cos(\tilde{\phi}_k - \tilde{\phi}_{k'})}. \tag{B17}$$

The term $|\frac{dh_1(\phi_k)}{d\phi_k}|^{-1} \times |\frac{dh_2(\phi_{k'})}{d\phi_{k'}}|^{-1}$, evaluated at $\phi_k = \tilde{\phi}_k + \phi_Q$ and $\phi_{k'} = \tilde{\phi}_{k'} + \phi_Q$, which we get according to Eq. (B11) from the two integrals in ϕ_k and $\phi_{k'}$, is given by

$$|h'_1(\tilde{\phi}_k + \phi_Q)|^{-1}|h'_2(\tilde{\phi}_k + \phi_Q)|^{-1} = \frac{1}{kk'|\sin(\tilde{\phi}_k - \tilde{\phi}_{k'})|}. \tag{B18}$$

Putting all together, we arrive at

$$\mathcal{B}^{n,j;J,N}_{m,\nu;m',\nu'} = \tilde{\mathcal{N}}_{n,j}\mathcal{N}_{J,N}\mathcal{N}_{m,\nu}\mathcal{N}_{m',\nu'}\frac{i^{m-m'+J+j}}{\rho_n^2}f(q,n,j)\frac{1}{kk'|\sin(\tilde{\phi}_k - \tilde{\phi}_{k'})|}e^{i(m\tilde{\phi}_k - m'\tilde{\phi}_{k'} - j\tilde{\phi}_q)}\int_0^{2\pi} d\phi_Q e^{i(m-m'-j-J)\phi_Q}. \tag{B19}$$

From this, we finally obtain the selection rule $\delta_{m-m',j+J}$ which expresses the conservation of angular momentum. Recalling that $k = k_{m,\nu}$, $k' = k_{m',\nu'}$, $Q = k_{J,N}$, we write as the final result

$$\mathcal{B}^{n,j;J,N}_{m,\nu;m',\nu'} = \delta_{m-m',j+J}\tilde{\mathcal{N}}_{n,j}\mathcal{N}_{J,N}\mathcal{N}_{m,\nu}\mathcal{N}_{m',\nu'}\frac{2\pi}{\rho_n^2}f(q,n,j)\frac{1}{k_{m,\nu}k_{m',\nu'}|\sin(\tilde{\phi}_k - \tilde{\phi}_{k'})|}e^{i(m\tilde{\phi}_k - m'\tilde{\phi}_{k'} - j\tilde{\phi}_q)}. \tag{B20}$$

The angles ϕ_k, $\phi_{k'}$, $\tilde{\phi}_q$ are defined in Eqs. (B14) and (B16). The value of q is given by Eq. (B17).

[1] W. Schäfer and M. Wegener, *Semiconductor Optics and Transport Phenomena*, 1st ed. (Springer, Berlin, 2002).

[2] H. Haug and S. W. Koch, *Quantum Theory of the Optical and Electronic Properties of Semiconductors*, 4th ed. (World Scientific, Singapore, 2004).

[3] C. Cohen-Tannoudji, J. Dupont-Roc, and G. Grynberg, *Atom-Photon Interactions* (Wiley, Weinheim, 1998).

[4] R. J. Elliott, Intensity of optical absorption by excitons, Phys. Rev. **108**, 1384 (1957).

[5] T. C. Berkelbach, M. S. Hybertsen, and D. R. Reichman, Bright and dark singlet excitons via linear and two-photon spectroscopy in monolayer transition-metal dichalcogenides, Phys. Rev. B **92**, 085413 (2015).

[6] G. Wang, X. Marie, I. Gerber, T. Amand, D. Lagarde, L. Bouet, M. Vidal, A. Balocchi, and B. Urbaszek, Giant Enhancement of the Optical Second-Harmonic Emission of WSe_2 Monolayers by Laser Excitation at Exciton Resonances, Phys. Rev. Lett. **114**, 097403 (2015).

[7] L. Allen, M. W. Beijersbergen, R. J. C. Spreeuw, and J. P. Woerdman, Orbital angular momentum of light and the transformation of Laguerre-Gaussian laser modes, Phys. Rev. A **45**, 8185 (1992).

[8] A. M. Yao and M. J. Padgett, Orbital angular momentum: origins, behavior and applications, Adv. Opt. Photon. **3**, 161 (2011).

[9] J.P. Torres and L. Torner, *Twisted Photons: Applications of Light with Orbital Angular Momentum* (Wiley, Weinheim, 2011).

[10] U. Bhattacharya, S. Chaudhary, T. Grass, A. S. Johnson, S. Wall, and M. Lewenstein, Fermionic Chern insulator from twisted light with linear polarization, Phys. Rev. B **105**, L081406 (2022).

[11] T. Graß, M. Gullans, P. Bienias, G. Zhu, A. Ghazaryan, P. Ghaemi, and M. Hafezi, Optical control over bulk excitations in fractional quantum Hall systems, Phys. Rev. B **98**, 155124 (2018).

[12] H. Fujita, Y. Tada, and M. Sato, Accessing electromagnetic properties of matter with cylindrical vector beams, New J. Phys. **21**, 073010 (2019).

[13] B. Cao, T. Grass, G. Solomon, and M. Hafezi, Optical flux pump in the quantum Hall regime, Phys. Rev. B **103**, L241301 (2021).

[14] H. Fujita and M. Sato, Encoding orbital angular momentum of light in magnets, Phys. Rev. B **96**, 060407(R) (2017).

[15] H. Fujita and M. Sato, Ultrafast generation of skyrmionic defects with vortex beams: Printing laser profiles on magnets, Phys. Rev. B **95**, 054421 (2017).

[16] Z.-P. Cian, T. Grass, A. Vaezi, Z. Liu, and M. Hafezi, Engineering quantum Hall phases in a synthetic bilayer graphene system, Phys. Rev. B **102**, 085430 (2020).

[17] H. Kim, H. Dehghani, I. Ahmadabadi, I. Martin, and M. Hafezi, Floquet vortex states induced by light carrying an orbital angular momentum, Phys. Rev. B **105**, L081301 (2022).

[18] C. T. Schmiegelow, J. Schulz, H. Kaufmann, T. Ruster, U. G. Poschinger, and F. Schmidt-Kaler, Transfer of optical orbital angular momentum to a bound electron, Nat. Commun. **7**, 12998 (2016).

[19] A. M. Konzelmann, S. O. Krüger, and H. Giessen, Interaction of orbital angular momentum light with Rydberg excitons:

Modifying dipole selection rules, Phys. Rev. B **100**, 115308 (2019).

[20] M. F. Andersen, C. Ryu, P. Cladé, V. Natarajan, A. Vaziri, K. Helmerson, and W. D. Phillips, Quantized Rotation of Atoms from Photons with Orbital Angular Momentum, Phys. Rev. Lett. **97**, 170406 (2006).

[21] M.-S. Kwon, B. Y. Oh, S.-H. Gong, J.-H. Kim, H. K. Kang, S. Kang, J. D. Song, H. Choi, and Y.-H. Cho, Direct Transfer of Light's Orbital Angular Momentum onto a Nonresonantly Excited Polariton Superfluid, Phys. Rev. Lett. **122**, 045302 (2019).

[22] G. F. Quinteiro and P. I. Tamborenea, Theory of the optical absorption of light carrying orbital angular momentum by semiconductors, Europhys. Lett. **85**, 47001 (2009).

[23] G. F. Quinteiro and P. I. Tamborenea, Twisted-light-induced optical transitions in semiconductors: Free-carrier quantum kinetics, Phys. Rev. B **82**, 125207 (2010).

[24] M. B. Farías, G. F. Quinteiro, and P. I. Tamborenea, Photoexcitation of graphene with twisted light, Eur. Phys. J. B **86**, 432 (2013).

[25] K. B. Simbulan, T.-D. Huang, G.-H. Peng, F. Li, O. J. G. Sanchez, J.-D. Lin, J. Qi, S.-J. Cheng, T.-H. Lu, and Y.-W. Lan, Selective photoexcitation of finite-momentum excitons in monolayer MoS_2 by twisted light, ACS Nano **15**, 3481 (2021).

[26] K. L. Seyler, P. Rivera, H. Yu, N. P. Wilson, E. L. Ray, D. G. Mandrus, J. Yan, W. Yao, and X. Xu, Signatures of moiré-trapped valley excitons in $MoSe_2/WSe_2$ heterobilayers, Nature (London) **567**, 66 (2019).

[27] K. Tran, G. Moody, F. Wu, X. Lu, J. Choi, K. Kim, A. Rai, D. A. Sanchez, J. Quan, A. Singh, J. Embley, A. Zepeda, M. Campbell, T. Autry, T. Taniguchi, K. Watanabe, N. Lu, S. K. Banerjee, K. L. Silverman, S. Kim *et al.*, Evidence for moiré excitons in van der Waals heterostructures, Nature (London) **567**, 71 (2019).

[28] C. Jin, E. C. Regan, A. Yan, M. Iqbal Bakti Utama, D. Wang, S. Zhao, Y. Qin, S. Yang, Z. Zheng, S. Shi, K. Watanabe, T. Taniguchi, S. Tongay, A. Zettl, and F. Wang, Observation of moiré excitons in WSe_2/WS_2 heterostructure superlattices, Nature (London) **567**, 76 (2019).

[29] E. M. Alexeev, D. A. Ruiz-Tijerina, M. Danovich, M. J. Hamer, D. J. Terry, P. K. Nayak, S. Ahn, S. Pak, J. Lee, J. I. Sohn, M. R. Molas, M. Koperski, K. Watanabe, T. Taniguchi, K. S. Novoselov, R. V. Gorbachev, H. S. Shin, V. I. Fal'ko, and A. I. Tartakovskii, Resonantly hybridized excitons in moiré superlattices in van der Waals heterostructures, Nature (London) **567**, 81 (2019).

[30] P. Cudazzo, I. V. Tokatly, and A. Rubio, Dielectric screening in two-dimensional insulators: Implications for excitonic and impurity states in graphane, Phys. Rev. B **84**, 085406 (2011).

[31] A. D. Jackson and L. C. Maximon, Integrals of products of Bessel functions, SIAM J. Math. Anal. **3**, 446 (1972).

[32] I. Strzalkowski, S. Joshi, and C. R. Crowell, Dielectric constant and its temperature dependence for GaAs, CdTe, and ZnSe, Appl. Phys. Lett. **28**, 350 (1976).

[33] A. Laturia, M. L. Van de Put, and W. G. Vandenberghe, Dielectric properties of hexagonal boron nitride and transition metal dichalcogenides: from monolayer to bulk, npj 2D Mater. Appl. **2**, 6 (2018).

[34] M. Cardona, Electron Effective Masses of InAs and GaAs as a Function of Temperature and Doping, Phys. Rev. **121**, 752 (1961).

[35] A. Kormányos, G. Burkard, M. Gmitra, J. Fabian, V. Zólyomi, N. D. Drummond, and V. Fal'ko, $\mathbf{k}\cdot\mathbf{p}$ theory for two-dimensional transitional metal dichalcogenide semiconductors, 2D Mater. **2**, 022001 (2015).

[36] C. Jörg, G. Queraltó, M. Kremer, G. Pelegrí, J. Schulz, A. Szameit, G. von Freymann, J. Mompart, and V. Ahufinger, Artificial gauge field switching using orbital angular momentum modes in optical waveguides, Light Sci. Appl. **9**, 150 (2020).

[37] C. Lagoin, S. Suffit, K. Baldwin, L. Pfeiffer, and F. Dubin, Mott insulator of strongly interacting two-dimensional semiconductor excitons, Nat. Phys. **18**, 149 (2022).

[38] C. Lagoin, U. Bhattacharya, T. Grass, R. Chhajlany, T. Salamon, K. Baldwin, L. Pfeiffer, M. Lewenstein, M. Holzmann, and F. Dubin, Checkerboard solid of dipolar excitons in a two-dimensional lattice, arXiv:2201.03311.

[39] A. Dhar, M. Maji, T. Mishra, R. V. Pai, S. Mukerjee, and A. Paramekanti, Bose-Hubbard model in a strong effective magnetic field: Emergence of a chiral Mott insulator ground state, Phys. Rev. A **85**, 041602(R) (2012).

[40] K. Suthar, H. Sable, R. Bai, S. Bandyopadhyay, S. Pal, and D. Angom, Supersolid phase of the extended Bose-Hubbard model with an artificial gauge field, Phys. Rev. A **102**, 013320 (2020).